

All-Glass 3D Optofluidic Microchip with Built-in Tunable Microlens Fabricated by Femtosecond Laser-Assisted Etching

Yanlei Hu, Shenglong Rao, Sizhu Wu, Pengfei Wei, Weixin Qiu, Dong Wu,* Bing Xu, Jincheng Ni, Liang Yang, Jiawen Li, Jiaru Chu, and Koji Sugioka*

Development of tunable microlenses by taking advantage of the physical adaptability of fluids is one of the challenges of optofluidic techniques, since it offers many applications in biochips, consumer electronics, and medical engineering. Current optofluidic tuning methods using electrowetting or pneumatic pressure typically suffer from high complexity involving external electromechanical actuating devices and limited tuning performance. In this paper, a novel and simple tuning method is proposed that changes the liquid refractive index in an optofluidic channel while leaving the shape of the microlens unchanged. To create an optofluidic microlens with high robustness and optical performance, built-in microlenses are fabricated inside 3D glass microfluidic channels by optimized single-operation wet etching assisted by a femtosecond laser. Tuning of focusing properties is demonstrated by filling the channel with media having different indices. Continuous tuning over a wide range (more than threefold tunability for both focal length and focal spot size) is also achieved by pumping sucrose solutions with different concentrations into the microchip channels. Reversible tuning is experimentally verified, indicating intriguing properties of the all-glass optofluidic microchip. Both the proposed tuning method and the all-glass architecture with built-in microlens offer great potential toward numerous applications, including microfluidic adaptive imaging and biomedical sensing.

1. Introduction

Optofluidics, taking advantage of the synergy of microfluidics and micro-optics, facilitates its wide applicability by providing a platform for generating and manipulating light on a microchip. Development of tunable optical systems based on the physical adaptability of fluids has long been one of the most important tasks in optofluidics research.^[1–4] As a fundamental element of optofluidics, the microlens affords a wide range of applications in microfluidic engineering, such as cell counting,^[5] optical trapping,^[6] and fluidic lasing and sensing.^[7] Development of a tunable microlens has recently attracted considerable attention due to its unique potential applications.^[8–13] A macroscale analogue is the zoom lens in a commercial camera, in which the focal length of the lens group can be changed by displacing the lens components along the axis parallel to the lens arrangement to realize autofocusing functionality for taking photos at different depths of field.

By benefiting from compact size, low light energy consumption, and high integration level, achieving tunability of microscale lenses would be advantageous for distinct implementations, such as adaptive plenoptic cameras, tissue endoscopes, and advanced solar concentrators.

Although the challenges of manageable control of the microlens shape and position remain unaccomplished, a certain degree of tunability has been achieved over the past decades.^[14,15] Electrowetting has emerged as an attractive way to control the shape of a liquid lens on a hydrophobic solid surface by electrostatically tuning the interfacial tension before solidification.^[16,17] However, the liquid used for the lens is limited to conductive and photosensitive materials, and a large optical aperture is extremely difficult to achieve. Furthermore, the process is accompanied by liquid evaporation.^[18] Meanwhile, liquid-filled microlenses placed inside a flexible polymeric chamber or between thin elastic membranes can vary their optical characteristics due to shape changes actuated by an external force, for example, periphery movement,^[19] fluidic pressure,^[20] or electromagnetic actuation,^[21] providing a wide range of tunability. However, external actuation devices such as mechanical pumps are required, and their operation is

Prof. Y. L. Hu, S. L. Rao, W. X. Qiu, Prof. D. Wu, B. Xu, J. C. Ni, L. Yang, Prof. J. W. Li, Prof. J. R. Chu
CAS Key Laboratory of Mechanical Behavior and Design of Materials
Department of Precision Machinery and Precision Instrumentation
University of Science and Technology of China
Hefei 230026, China
E-mail: dongwu@ustc.edu.cn

Prof. S. Z. Wu
Department of Mechanical and Electronic Engineering
Hefei University of Technology
Hefei 230009, China

Prof. P. F. Wei
Department of Physics
Shaoxing University
Shaoxing 312000, China

Prof. K. Sugioka
Laser Technology Laboratory
RIKEN
2-1 Hirosawa, Wako, Saitama 351-0198, Japan
E-mail: ksugioka@riken.jp

DOI: 10.1002/adom.201701299

complicated, hindering their integration into a compact microchip. An adaptive refractive lens has been demonstrated by employing bi-phase emulsion droplets of two immiscible solutions and controlling the curvature of the meniscus.^[22] The droplet compound microlenses, however, remain in a liquid state, making them difficult to work with in microfluidic environments and sensitive to external stimuli, for example, chemicals or vibration. In addition, dynamic and reversible tuning of optical properties has not yet been achieved.

Another effective approach to optical tunability is to control the refractive index contrast between the lenses and the surrounding media. Liquid crystal (LC) lenses are typically used as tunable refractive optical elements, and they have been intensively studied by generating an electric field gradient within the LC layer.^[23] However, accurate control of the electric field distribution is a difficult task, and additional elements, such as a power supply and patterned metallic electrodes, are needed, increasing the complexity of the microchip design. Overall, the tunability of reported micro-optofluidic lenses so far can be categorized into two main types: tunability with lens liquid and tunability with lens shape.^[13] Each way has its own disadvantages for practical applications. Development of a robust optofluidic microlens with simple tuning method is highly in demand.

In contrast, immersing a lens in liquids with different refractive indices leads to convenient tuning of the microlens without external actuators or voltages. With this method, what is needed is a microlens fabricated inside a closed microfluidic channel. Femtosecond laser direct writing is a powerful technology for the fabrication of flexible 3D microstructures in a customizable manner.^[24–29] Previously, our group has reported a “ship-in-a-bottle” femtosecond laser integration of 3D microoptical devices in a channel.^[30,31] First, a 3D glass microchannel is filled with a photosensitive polymer, and then two-photon polymerization is used to form the optical element. However, integrated polymeric microoptical devices cannot be used in harsh environments owing to their poor thermal and mechanical stability and low chemical and moisture resistance.^[8,32,33] Glass is more reliable for constructing microlenses due to its stable chemical and physical properties, which can diversify the applications. Nevertheless, processing of glass is more complicated, time-consuming, and expensive than polymer processing. Particularly, it is challenging to produce glass with the high surface quality demanded by high-precision optical components.

In this paper, we report a 3D optofluidic system with built-in all-glass microlenses that have reversible tunability by varying the liquid refractive index within a microfluidic channel over time. Unlike other methods, the refractive index and shape of the microlenses remain unchanged, while the refractive index contrast is altered by changing the media that surrounds them, thereby achieving optofluidic tuning of the focusing properties, as illustrated in **Figure 1**. An all-glass optofluidic structure with good robustness, stability, and optical performance is facilitated by femtosecond laser-assisted etching (FLAE). Another advantage of FLAE is that it can create the all-glass optofluidics structure in a single operation without any other methods. The fabrication process has been optimized to ensure high quality of the glass surface profile. The FLAE enabled fabrication of microlenses on a flat surface and an open channel and even in embedded closed channels, whose corresponding optical

focusing and imaging properties were characterized. Different kinds of liquids with different refractive indices (water, ethanol, and sucrose solution) and sucrose solution with different concentrations were used to tune the optofluidic microlens. Wide tunability of focal length (from 260 to 2,450 μm) and focal spot size (from 6.8 to 59.5 μm) were experimentally demonstrated.

2. Results and Discussion

2.1. Simulation of Focusing Properties of 3D Optofluidic Microlens

Both the finite-difference time-domain (FDTD) method and analytic scalar diffraction calculation can be adopted to simulate the light intensity distribution focused by the glass microlens. For FDTD simulations, the geometric parameters of the designed optofluidic microlens and the optical refractive indices of the photosensitive glass and liquid are the main input parameters. A 3D model was built and the minimum mesh cell (conformal refined) was carefully chosen to reach reasonably accurate results within an acceptable calculation time. Perfectly matched layer boundary conditions were applied at the edge of the simulation region. A plane wave source with a wavelength from 400 to 700 nm was selected as the incident beam to simulate the white light. The light intensity at the focus was captured by a frequency domain profile monitor (Figure 1c,d). For the scalar diffraction calculation method, a triple-fast Fourier transform (TFFT) algorithm was used for calculating Fresnel diffraction. We define the impulse response function as

$$\tilde{h} = \frac{\exp(jkd)}{j\lambda d} \exp\left[\frac{jk}{2d}(x^2 + y^2)\right] \quad (1)$$

where λ is the wavelength, k is the wavenumber, and d is the distance between the diffraction and observation planes. According to the spatial invariance of the impulse response of Fresnel diffraction, the Fresnel diffraction formula can be written in a convolution form

$$\begin{aligned} \tilde{U}(x, y) &= \tilde{U}_0(x_0, y_0) \otimes \tilde{h}(x, y) \\ &= \frac{\exp(jkd)}{j\lambda d} \times \left\{ \tilde{U}_0(x_0, y_0) \otimes \exp\left[\frac{jk}{2d}(x^2 + y^2)\right] \right\} \end{aligned} \quad (2)$$

where $\tilde{U}_0(x_0, y_0)$ is the optical complex amplitude distribution of the diffraction plane determined by the lens profile and $\tilde{U}(x, y)$ is the optical complex amplitude distribution of the observation plane.

Therefore, one can complete the calculation of Equation (2) by performing two Fourier transforms and one inverse Fourier transform (i.e., first transforming to the frequency domain and then transforming back to the space domain)

$$\tilde{U}(u, v) = \text{FFT}\{\tilde{U}_0(x_0, y_0)\} \times \text{FFT}\left\{\exp\left[\frac{jk}{2d}(x^2 + y^2)\right]\right\} \quad (3)$$

$$\tilde{U}(x, y) = \frac{\exp(jkd)}{j\lambda d} \times \text{FFT}^{-1}\{\tilde{U}(u, v)\} \quad (4)$$

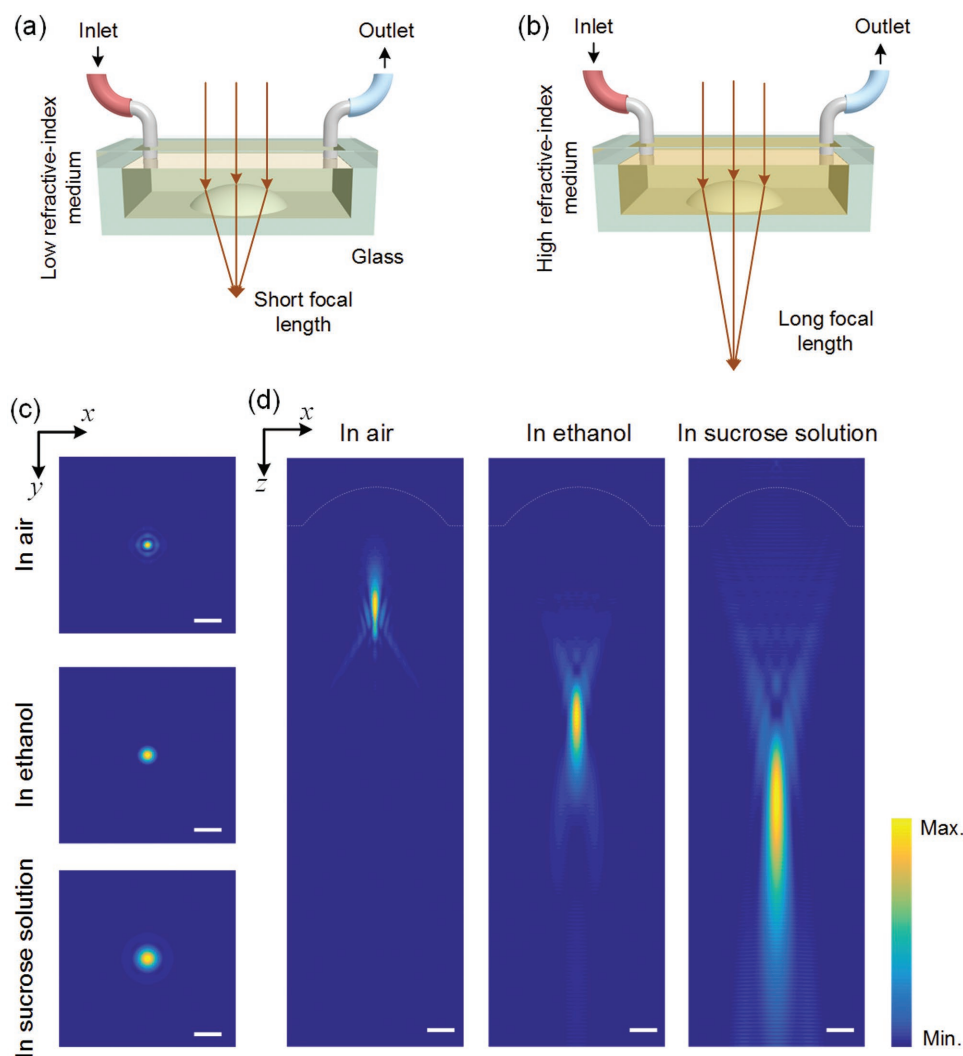


Figure 1. Optofluidic tunable microlens with the aid of changeable liquids with different refractive indices. a,b) Schematic diagrams of the concept of an optofluidic tunable microlens. By filling the channel with different media, the refractive index contrast changes to control the focusing characteristics. c) Simulation results for the focal spots by a glass lens in air ($n = 1$), ethanol ($n = 1.362$), and 50% sucrose solution ($n = 1.422$). The glass spherical microlens used for simulation has a base diameter of $140\ \mu\text{m}$ and height of $30\ \mu\text{m}$. d) Cross-sectional profiles of the focus fields along the light propagation. Scale bars: $20\ \mu\text{m}$.

2.2. Optimal Design and Fabrication of Glass Microlens by FLAE on Flat Surfaces

The mechanism of FLAE is based on the fact that the laser irradiation of photosensitive glass produces a much higher HF etching rate in the irradiated areas with respect to unexposed areas. The higher etching rate is due to the growth of crystalline phase of lithium metasilicate around silver nanoparticles precipitated within the irradiated region resulting from reducing reaction with free electrons generated by nonlinear multiphoton absorption and successive annealing. **Figure 2a** is a schematic illustration of the fabrication of the glass microlens by FLAE on a flat glass surface. The femtosecond laser is first employed to scan the photosensitive glass in a programmed pattern. In general, a line-by-line scanning mode is used for generating 3D functional structures inside photosensitive glass. Here, an optimal circular scanning

mode is applied for fabrication in order to better match the profile of the spherical microlens. Driven by a nanopositioning stage, the glass sample is scanned by the laser focus along the route of a series of concentric circles with a fixed pitch. The scanning pitch is crucial for achieving high surface quality for optical applications, with a smaller scanning pitch resulting in a smoother surface. However, the fabrication time increases greatly with the reduction of the scanning pitch. In our experiments, $4\ \mu\text{m}$ was found to be an optimal value for the scanning pitch that not only ensured a highly smooth microlens surface but also reduced the fabrication time effectively (**Figure 2b** and **Figure S1**, Supporting Information). For example, for a microlens with a diameter of $200\ \mu\text{m}$ and height of $50\ \mu\text{m}$, the scanning time was only 65 s with a constant laser scanning speed of $1000\ \mu\text{m}\ \text{s}^{-1}$. The laser power of 5 mW was selected after a series of fabrication and optical tests under a microscope.

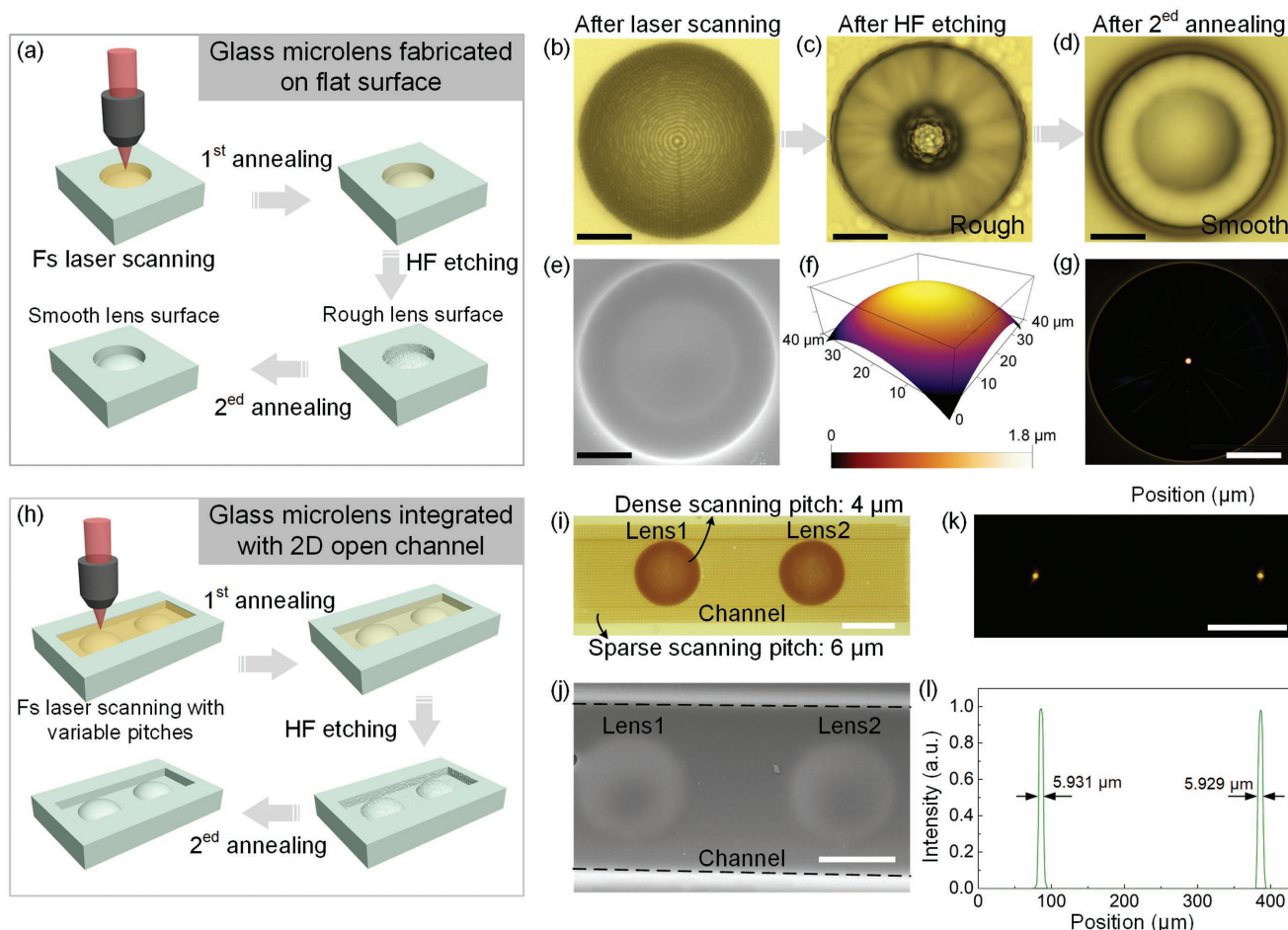


Figure 2. Fabrication of glass microlens and integration of microlens into open microchannel by single FLAE operation. a) Schematic illustration of the fabrication of a microlens on a flat glass surface. Optical microscopy images of the glass microlens at different steps: b) after laser scanning, c) after HF etching, and d) after the second annealing. e) SEM image of the prepared microlens. f) AFM topography characterization of the prepared microlens. Note that only a region of $40\ \mu\text{m} \times 40\ \mu\text{m}$ on the top of the microlens is measured due to the limitation of the AFM scanning range. g) Focusing image of the glass microlens in air. Scale bars: $50\ \mu\text{m}$. h) Schematic illustration of the fabrication procedure for glass microlens integrated into the microchannel. i) Optical microscopy image of the glass microlens integrated into microchannel after laser scanning. j) SEM image of the microlens in the microchannel. k–l) Focusing characteristics of the glass microlens in a microchannel in air. Scale bars: $100\ \mu\text{m}$.

After laser scanning, the sample was subjected to the first annealing and HF etching for 1 h. This created a 3D microlens with poor surface smoothness (Figure 2c). To improve the surface smoothness, the sample was subjected to the second annealing at an optimized temperature of $645\ \text{°C}$ (higher than the $570\ \text{°C}$ applied in previous work^[34]). Higher annealing temperatures ($>680\ \text{°C}$) resulted in severe deformation of the microchannel in previous experiments.

Figure 2d,e shows optical microscopy image and scanning electron microscopy (SEM) image of the prepared microlens after the optimized second annealing. Compared with Figure 2c, the surface quality is greatly improved, as further verified by the surface profile measured by atomic force microscopy (AFM) in Figure 2f. Furthermore, according to the AFM characterization (Figure S2, Supporting Information), the surface profile of as-prepared microlens agrees well with the designed spherical profile. After subtracting the whole surface spherical topography, the rms roughness of the microlens surface is $10.6\ \text{nm}$, which is far below the visible light wavelength. Figure 2g

shows the image of the focusing spot, indicating tight focusing characteristic with a spot size of $4.52\ \mu\text{m}$ using the microlens prepared at the glass surface.

2.3. Integration of Glass Microlens into Open Channels by Single Operation FLAE

Due to the good programmability of the laser fabrication facility, not only a single 3D complex lens structure but also 3D microchannel structures can be fabricated by a single laser operation without additional processes. Figure 2h illustrates the schematic fabrication process of a couple of microlenses in an open channel. A long channel with a millimeter scale or longer is commonly needed for practical optofluidic applications, but creation of such a channel takes an unacceptably long time with femto-second laser scanning. Here, we developed an adaptive scanning strategy for fabricating glass microlenses integrated into the channel by combining dense and sparse scanning modes.

As mentioned above, a smaller scanning pitch results in better surface quality. Dense scanning with a small pitch of 4 μm was adopted for fabricating the microlens, which requires a smoother surface. In contrast, the channel typically does not require high optical quality, so a sparse scanning with a pitch of 6 μm could be applied. In this way, the fabrication time was reduced to 11 min for creating an optofluidic chip comprising a couple of microlenses and a channel with a height of 200 μm and a length of 2 mm. In Figure 2i, the dense scanning area appears to be darker than the sparse scanning area. Figure 2j shows an SEM image of the fabricated microlenses and channel, verifying the high surface quality of the optical components. Figure 2k shows an optical microscopy image of the focal spots of the microlens array, which exhibits good uniformity of the focus intensities produced by each lens. Specifically, by evaluation of the spatial intensity distribution shown in Figure 2l, we can see that the two foci have almost the same intensity and size (5.931 and 5.929 μm), which further validates the high reproducibility of our method for manufacturing optofluidic devices.

2.4. Performance of Optofluidic Microlenses with Closed Channel and Refractive Index Tuning

When microoptical elements are integrated into an open channel, a flexible cover membrane (e.g., polydimethylsiloxane) has to be applied to close the channel for optofluidic applications. Additional bonding and sealing processes are needed that increase the fabrication complexity and lower the integration level of the device. By taking advantage of the 3D fabrication ability and programmability of FLAE, all-glass 3D optofluidic structures with built-in microlenses and closed microchannels can be readily fabricated.

Figure 3a shows a schematic diagram of microlens fabrication in a closed glass microchannel by FLAE. Adaptive scanning is also adopted for this fabrication process, as described in the previous section. Figure 3b shows an optical microscopy image of the fabricated optofluidic microchip after laser scanning, from which we can see that the scanning pitch for fabricating the channel is sparser than that for fabricating the microlens. The optofluidic microchip was designed to have four glass microlenses, referred to as Lens 1, Lens 2, Lens 3, and Lens 4, with different sizes of 140, 160, 220, and 250 μm , respectively, inside two closed channels. The height of all lenses is designed to be the same, 50 μm . For fluid pumping, two common cubic reservoirs are arranged to connect the ends of the two microchannels. Figure 3c shows the prepared optofluidic microchip after HF etching and the second annealing; it exhibits good consistency in geometry corresponding to the laser scanning pattern.

The all-glass built-in structure of the optofluidic system provides overriding advantages, including high mechanical robustness and good resistance to harsh environments involving chemicals. To demonstrate the optical tunability of the optofluidic microlens, the focal spot size and focal length were tested in air, ethanol, and sucrose solution. These three media have different refractive indices: $n_{\text{air}} = 1$, $n_{\text{ethanol}} = 1.362$, and $n_{\text{sucrose}} = 1.402$ at a mass ratio of 40% – while the refractive index of Foturan glass is $n_g = 1.515$. As shown in Figure 3d–f,

the sizes of the focal spots can be tuned over a wide range by changing the channel liquids. The focal spot size increased with increasing microlens diameter, as the lens heights are the same and a larger diameter results in a smaller numerical aperture. The focal spot size also increases with increasing refractive index of the channel media because the refractive index contrast decreases and thus reduces the numerical aperture.

Figure 3g,h shows quantitative comparisons of the focal spot sizes and focal lengths of the microlenses in different media, verifying that the proposed concept of optical tuning by changing the channel media without external chemical or electrical stimuli. Besides the focusing test, an imaging characterization was also carried out as shown in Figure 3i–k. Due to different focal lengths, the input patterns were imaged at different positions for each lens. By moving the microchip vertically, the imaged patterns appeared to sharpen gradually one by one (Figure S3, Supporting Information). More imaging examples are shown in Figure S4 (Supporting Information). The sizes of the images naturally changed with the same principle as focusing. The contrast of the imaging pattern decreased with increasing size due to the unchanged total incident light intensity.

2.5. Continuous and Reversible Tuning of Optical Properties of Optofluidic Microlens in Sucrose Solutions

The refractive index of sucrose solution can be continuously tuned by gradually changing its concentration,^[35] providing us with a promising platform for optofluidic applications by facilely tailoring the optical properties. According to our measurements (by Abbe refractometer), the refractive index of the sucrose solution increased linearly with the mass ratio, as shown in Figure 4a. A wide range of refractive indices from 1.33 (pure water) to 1.452 ($\omega = 64\%$) could be achieved. By changing the concentration of the sucrose solution in the optofluidic microchip, continuous tuning of the focal length and focal spot size could be accomplished. The measured focal lengths are shown in Figure 4b, and they are consistent with the calculated values (Figure S5, Supporting Information). A Fresnel diffraction-based scalar method was applied to calculate the focusing field of the microlens in different media (details can be seen in Figure S6, Supporting Information). Figure 4c shows the foci of the four different glass microlenses in sucrose solutions with different concentrations, which agree well with the simulated results (Figure S7, Supporting Information). Lens 1, for example, shows that the focal spot size and focal length could be tuned from 6.8 to 21.6 μm and from 260 to 800 μm , respectively (Figure 4b–d). For Lens 4, they could be tuned from 19.9 to 59.5 μm , and from 800 to 2450 μm , respectively. This represents a threefold tunability for both the focal spot size and the focal length. The demonstrated results show good continuous tunability of the all-glass built-in structure with the optofluidic method, exhibiting great potential in the application fields where wide-range tuning is needed, for example, 3D light field camera or programmable cell-detection microchips.

The tuning of the microlens optical properties is reversible because of the robustness of the glass device and its facile operation. Here, we measured the focal length change of

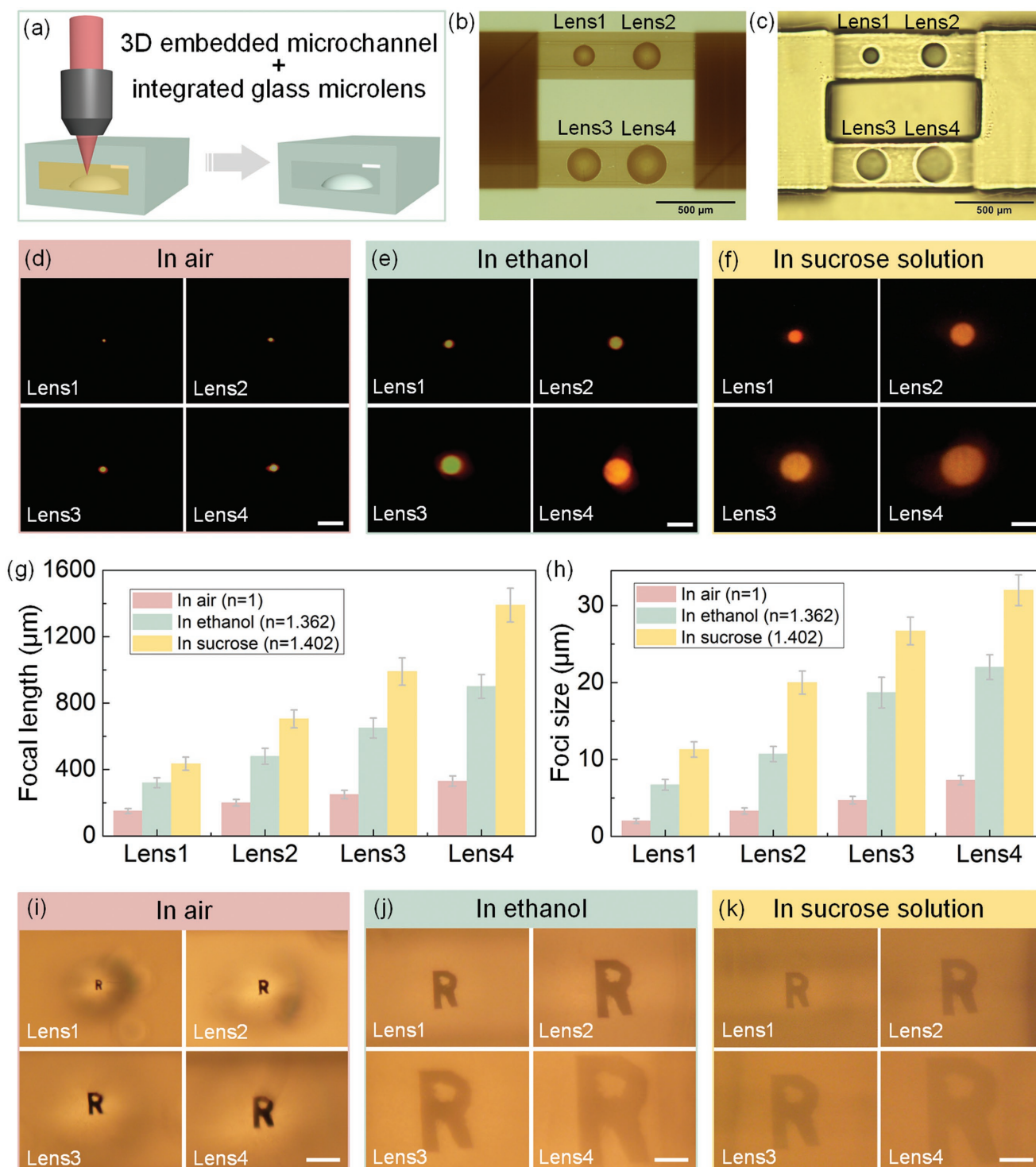


Figure 3. Fabrication and optical characterization of optofluidic microlens integrated in closed microchannels. a) Schematic illustration of the fabrication of a microlens integrated into a closed microchannel. Optical microscopic images of fabricated optofluidic microchip consisting of four glass microlenses with different sizes inside closed microchannels: b) after laser scanning and c) after the second annealing. d–f) Optical microscopic images of the focal spots produced by the microlenses in air, ethanol, and sucrose solution, respectively. Scale bars: 20 μm . g, h) Quantitative comparison of focal length and focal spot size for four microlenses in different aqueous solutions. i–k) Optical imaging characterization of the microlenses in air, ethanol, and sucrose solution, respectively. Scale bars: 20 μm .

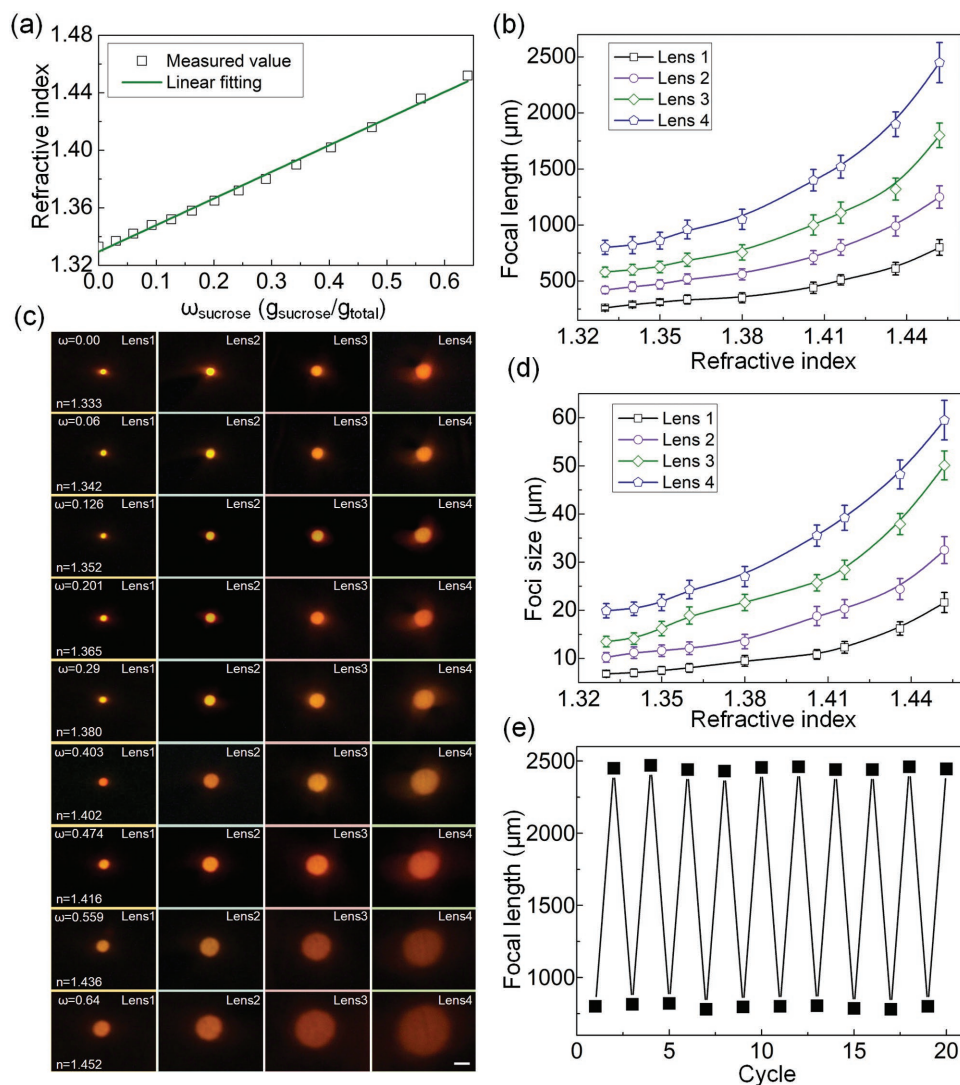


Figure 4. Continuous and reversible focus tuning of optofluidic microlenses in sucrose solutions. a) Variation in refractive index as a function of sucrose concentration. b) Dependence of the focal length of different microlenses on the refractive index for different sucrose concentration. c) Optical microscopy images of foci produced by different microlenses in different sucrose concentrations (mass ratios from $\omega = 0$ to $\omega = 0.64$). Scale bar: 20 μm . d) Dependence of the focal spot size for different microlenses on the refractive index of sucrose solutions. e) Reversible tuning of the optical properties by alternating sucrose solution and water in the microchannel.

Lens 4 by alternately filling the channel with pure water and sucrose solution ($\omega = 64\%$). Good reversibility can be seen from the result (Figure 4e). Furthermore, due to the scalability of FLAE, not only a glass lens with microscale dimensions but also a larger lens with a diameter of millimeters, can be fabricated in the same manner (Figure S8, Supporting Information), extending the applications of the optofluidic tunable devices.

3. Conclusion

In conclusion, we reported the fabrication of an all-glass optofluidic microchip with built-in microlenses by means of FLAE. The fabrication process was optimized to achieve good surface quality of the glass microlens with high efficiency. The microlenses and microchannels prepared by a single FLAE operation

exhibited good robustness, stability, and optical performance. Compared with other conventional microfabrication techniques (e.g., photolithography), FLAE features the advantages of real 3D capability, applicability to rigid brittle materials, and simple procedure. An innovative tuning method was also demonstrated by changing the refractive index of the medium in the optofluidic channel, while the shape and refractive index of glass microlenses remained unchanged. Optofluidic tuning of microlenses was demonstrated by pumping water, ethanol, and sucrose solution into the closed microfluidic channels. Continuous tuning over a wide range was also achieved by using sucrose solutions with different concentrations. The method has the advantages of simplicity and reversibility, without the need for external chemical and electrical actuation. The proposed fabrication of all-glass built-in optofluidic microlens and tuning of optical properties by

manipulating the refractive indices might open a new avenue for numerous applications including 3D tomographic imaging and biomedical in situ sensing.

4. Experimental Section

Laser Fabrication: The femtosecond laser used for FLAE has a 522 nm wavelength produced by second-harmonic generation from an amplified Yb-doped fiber laser (FCPA μ Jewel D-400, IMRA America, with a central wavelength of 1045 nm, a pulse width of 360 fs, and a repetition rate of 200 kHz). Commercial photosensitive glass (Foturan, Schott Glass Corp., Germany) consisting of lithium aluminosilicate doped with trace amounts of silver, cerium, sodium, and antimony was used for fabrication of the all-glass optofluidic structure.^[36] The photosensitive glass was directly irradiated by a femtosecond laser with a programmable scanning pattern through an objective lens (20 \times , NA 0.46). The microchannel and microlens were created by a single FLAE operation. The scanning pitch was chosen to strike a balance between fabrication time and surface smoothness. A tighter scanning pitch resulted in smoother channel walls and lens surface but leads to a longer fabrication time, as shown in Figure S1 (Supporting Information).

Annealing and Wet Etching: After laser scanning, the Foturan glass was annealed in a programmable furnace in order to form a crystalline phase of lithium metasilicate. The temperature was controlled in four stages: first increased to 500 °C at a rate of 5 °C min⁻¹, held constant for 1 h, raised to 605 °C at a rate of 3 °C min⁻¹, and finally held constant for 1 h again. After the first annealing, the glass was put into an aqueous solution of 10% hydrofluoric acid (HF) in an ultrasonic bath for wet chemical etching to selectively remove the crystalline phase area, which has an \approx 50 times higher etching rate than the nonmodified regions. In order to increase the smoothness of the microchip structures, the glass was then subjected to a second annealing with three stages: the temperature was increased to 500 °C at a rate of 5 °C min⁻¹, then raised to 645 °C at a rate of 3 °C min⁻¹, and finally held constant for 1 h. Ultimately, the all-glass 3D optofluidic structure comprising integrated microlenses and embedded microfluidic channel was accomplished with high smoothness.

Optical Characterization: A pump-assisted optical characterization system (sketched in Figure S9, Supporting Information) to measure the optical performance of the integrated 3D optofluidic system was built. The characterization system consists of two parts: the optical system and pump system. The optical system contains a halogen lamp, charge-coupled device (CCD) camera, nanopositioning stage, objective lenses, and monitor. The pump system contains a pump and several thin plastic tubes. The white light emitted from the halogen lamp provides a coupling-free beam, which is promising for cell detection and counting. The focal spots or imaging patterns were magnified by the objective lens and then captured in situ by the CCD camera. For imaging tests, a mask with character-shaped apertures was placed above the halogen lamp and the characters were imaged by the optofluidic microlens. The pump was utilized to generate a negative pressure in the 3D optofluidic chamber to draw solutions with different refractive indices into the microchannel. The flow speed was controlled from 0 to 5 mm s⁻¹ by regulating the negative pressure. The focal spot size was directly measured from the images captured by the CCD camera. In order to quantitatively measure the focal length of the optofluidic microlens, the objective lens was first focused on the bottom surface of the channel to observe the position of the back plane of the lens. Then, the sample on the nanopositioning stage was driven down until the objective lens could obtain the focal spots sharply with maximum intensity. The distance between these two positions was regarded as the focal length of the microlens.

Supporting Information

Supporting Information is available from the Wiley Online Library or from the author.

Acknowledgements

This work was supported by the National Natural Science Foundation of China (Nos. 51675503, 61675190, 61475149, 51405464, 51605463, and 11474223), the Fundamental Research Funds for the Central Universities (No. WK2480000002), Chinese Academy of Sciences Instrument Project (YZ201566), “Chinese Thousand Young Talents Program,” and Youth Innovation Promotion Association CAS (2017495).

Conflict of Interest

The authors declare no conflict of interest.

Keywords

femtosecond lasers, microfabrication, microlenses, optofluidics, wet etching

Received: December 1, 2017

Revised: January 17, 2018

Published online: February 28, 2018

- [1] D. Psaltis, S. R. Quake, C. Yang, *Nature* **2006**, *442*, 381.
- [2] C. Monat, P. Domachuk, B. Eggleton, *Nat. Photonics* **2007**, *1*, 106.
- [3] H. Schmidt, A. R. Hawkins, *Nat. Photonics* **2011**, *5*, 598.
- [4] T. Nisisako, T. Ando, T. Hatsuzawa, *Small* **2014**, *10*, 5116.
- [5] L. Miccio, P. Memmolò, F. Merola, P. Netti, P. Ferraro, *Nat. Commun.* **2015**, *6*, 6502.
- [6] M. Werner, F. Merenda, J. Piguet, R.-P. Salathé, H. Vogel, *Lab Chip* **2011**, *11*, 2432.
- [7] H. Zhang, X. Wang, J. Wu, *Small* **2012**, *8*, 3775.
- [8] D. Liang, A. K. Agarwal, D. J. Beebe, H. Jiang, *Nature* **2006**, *442*, 551.
- [9] X. Zhang, N. Gao, Y. He, S. Liao, S. Zhang, Y. Wang, *Small* **2016**, *12*, 3788.
- [10] X. Ye, F. Zhang, Y. Ma, L. Qi, *Small* **2015**, *11*, 1677.
- [11] X. Zhang, N. Gao, Y. He, S. Liao, S. Zhang, Y. Wang, *Small* **2016**, *12*, 3788.
- [12] Y. Yang, X. Huang, X. Zhang, F. Jiang, X. Zhang, Y. Wang, *ACS Appl. Mater. Interfaces* **2016**, *8*, 8849.
- [13] N. Nguyen, *Biomicrofluidics* **2010**, *4*, 031501.
- [14] X. Mao, J. R. Waldeisen, B. K. Juluri, T. J. Huang, *Lab Chip* **2007**, *7*, 1303.
- [15] X. Mao, S.-C. S. Lin, M. I. Lapsley, J. Shi, B. K. Juluri, T. J. Huang, *Lab Chip* **2009**, *9*, 2050.
- [16] S. Yang, T. N. Krupenkin, P. Mach, E. A. Chandross, *Adv. Mater.* **2003**, *15*, 940.
- [17] S. Kuiper, B. Hendriks, *Appl. Phys. Lett.* **2004**, *85*, 1128.
- [18] T. Krupenkin, S. Yang, P. Mach, *Appl. Phys. Lett.* **2003**, *82*, 316.
- [19] H. Ren, S.-T. Wu, *Appl. Phys. Lett.* **2005**, *86*, 211107.
- [20] D.-Y. Zhang, N. Justis, Y.-H. Lo, *Appl. Phys. Lett.* **2004**, *84*, 4194.
- [21] S. W. Lee, S. S. Lee, *Appl. Phys. Lett.* **2007**, *90*, 121129.
- [22] S. Nagelberg, L. D. Zarzar, N. Nicolas, K. Subramanian, J. A. Kalow, V. Sresht, D. Blankschtein, G. Barbastathis, M. Kreysing, T. M. Swager, *Nat. Commun.* **2017**, *8*, 14673.
- [23] H. Ren, S.-T. Wu, *Opt. Express* **2006**, *14*, 11292.
- [24] R. R. Gattass, E. Mazur, *Nat. Photonics* **2008**, *2*, 219.
- [25] M. Malinauskas, A. Žukauskas, S. Hasegawa, Y. Hayasaki, V. Mizeikis, R. Buividas, S. Juodkazis, *Light: Sci. Appl.* **2016**, *5*, e16133.

- [26] Y. Hu, Z. Lao, B. P. Cumming, D. Wu, J. Li, H. Liang, J. Chu, W. Huang, M. Gu, *Proc. Natl. Acad. Sci. USA* **2015**, *112*, 6876.
- [27] Y. Hu, D. Wu, J. Li, W. Huang, J. Chu, *Opt. Express* **2016**, *24*, 23557.
- [28] Y. L. Sun, W. F. Dong, R. Z. Yang, X. Meng, L. Zhang, Q. D. Chen, H. B. Sun, *Angew. Chem., Int. Ed.* **2012**, *51*, 1558.
- [29] Y. Hu, Y. Chen, J. Ma, J. Li, W. Huang, J. Chu, *Appl. Phys. Lett.* **2013**, *103*, 141112.
- [30] D. Wu, L.-G. Niu, S.-Z. Wu, J. Xu, K. Midorikawa, K. Sugioka, *Lab Chip* **2015**, *15*, 1515.
- [31] D. Wu, J. Xu, L.-G. Niu, S.-Z. Wu, K. Midorikawa, K. Sugioka, *Light: Sci. Appl.* **2015**, *4*, e228.
- [32] K.-S. Hong, J. Wang, A. Sharonov, D. Chandra, J. Aizenberg, S. Yang, *J. Micromech. Microeng.* **2006**, *16*, 1660.
- [33] C. Zheng, A. Hu, K. D. Kihm, Q. Ma, R. Li, T. Chen, W. W. Duley, *Small* **2015**, *11*, 3007.
- [34] Y. Cheng, K. Sugioka, K. Midorikawa, *Opt. Express* **2005**, *13*, 7225.
- [35] E. Martinsson, M. M. Shahjamali, N. Large, N. Zeraee, Y. Zhou, G. C. Schatz, C. A. Mirkin, D. Aili, *Small* **2016**, *12*, 330.
- [36] D. Wu, S. Z. Wu, J. Xu, L. G. Niu, K. Midorikawa, K. Sugioka, *Laser Photonics Rev.* **2014**, *8*, 458.